REE + Y DISTRIBUTION IN TREMADOCIAN SHELLY PHOSPHORITES (TOOLSE, ESTONIA)

MULTI-STAGES ENRICHMENT IN SHALLOW MARINE ENVIRONMENT DURING EARLY DIAGENESIS

Sophie GRAUL, Ph.D. Candidate

Rutt HINTS, Toivo KALLASTE, Siim PAJUSAAR, Mawo N'DIAYE
Department of Geology – Mineral Resources

TALLINN UNIVERSITY OF TECHNOLOGY

THE GEOLOGICAL SOCIETY OF AMERICA®
CONNECTS 2022
9–12 October
Denver, Colorado, USA
& Online Everywhere

Estonian Research Council

GEOLOGICAL SETTING

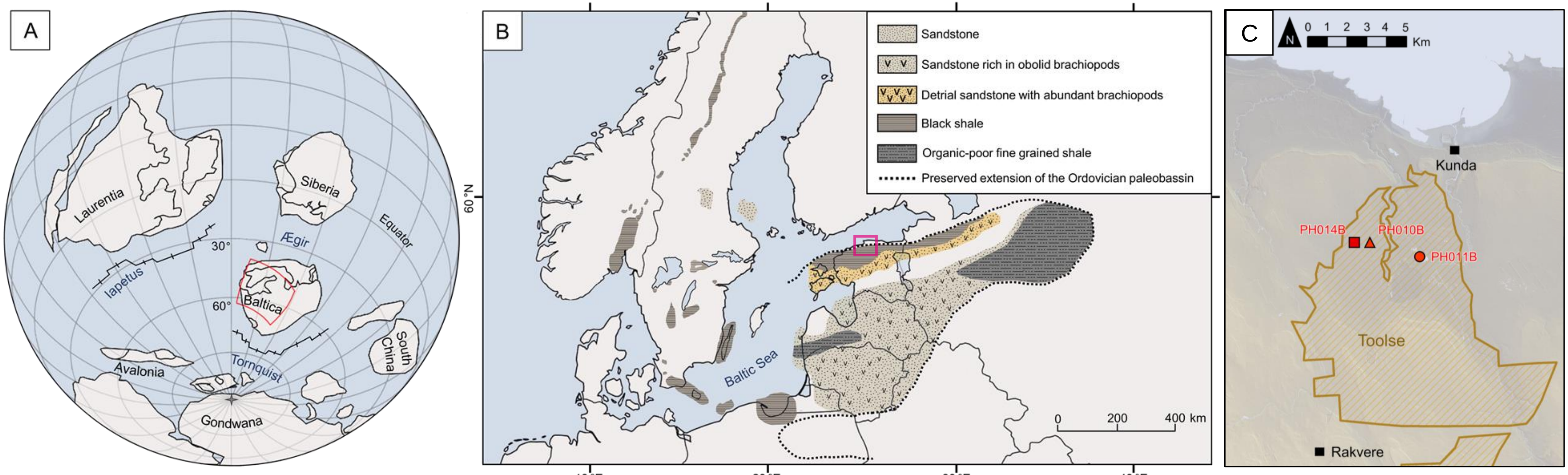

A) Early Ordovician relative position of the main paleocontinents, after Cocks & Torsvik [1]. B) Lithology of the preserved extension of the Ordovician Paleobassin in Baltic and Scandinavia, after Popov et al. [2]. C) Drill cores location in the Toolse deposit.

- Tremadocian sedimentary formation (485.4 to 477.7Ma), spread over the Baltic Ordovician paleobassin.
- Extension of shelly phosphorite deposits from Estonia to NW Russia, from the Pakerort stage (equal of Gasconadian stage).
- Kallavere formation: sandstone with abundant phosphatic brachiopods detritus related to coastal upwelling zones and deposited in shallow, coastal environment of a peritidal sea. Largest phosphate reserve in Europe, 3 billon metric tons [3].

GEOLOGICAL SETTING AND ANALYZE PLAN

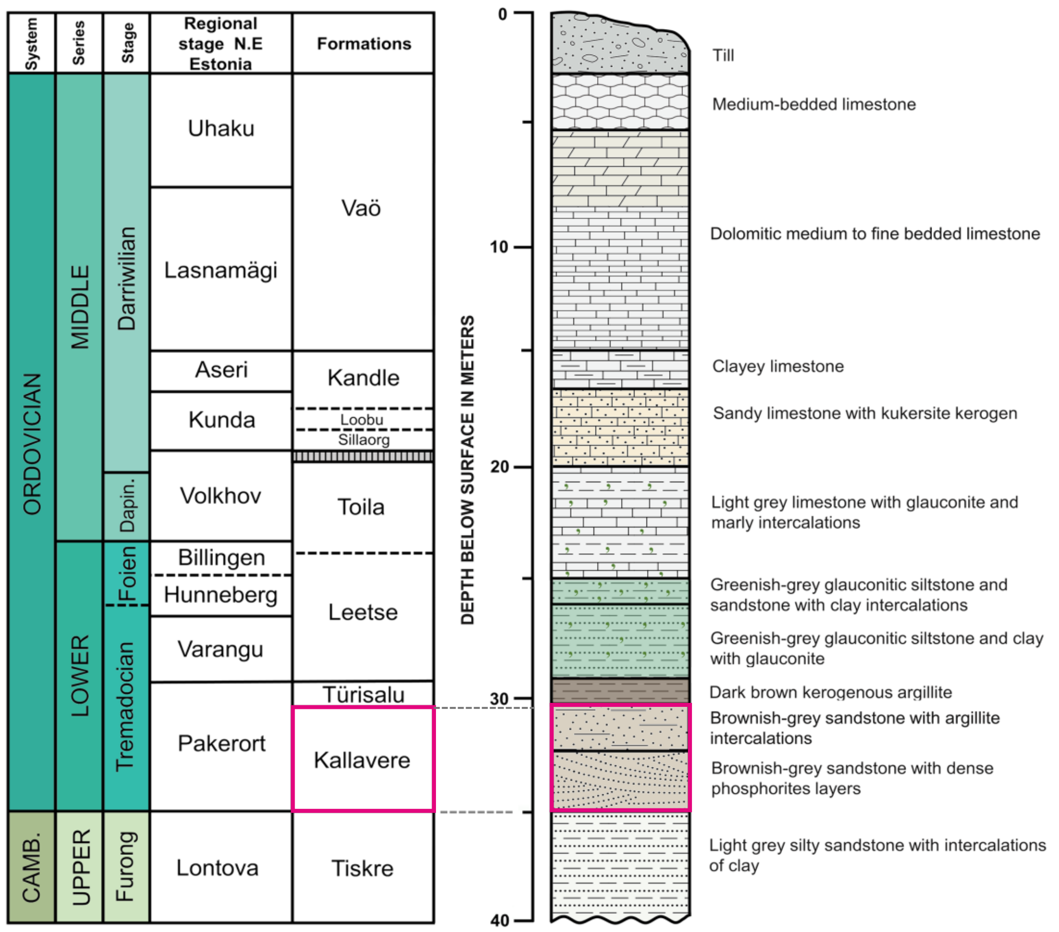

General stratigraphy and cross section of the Toolse deposit, with detail of the Kallavere Formation, regional stratigraphy after Nõlvak et al. [4].

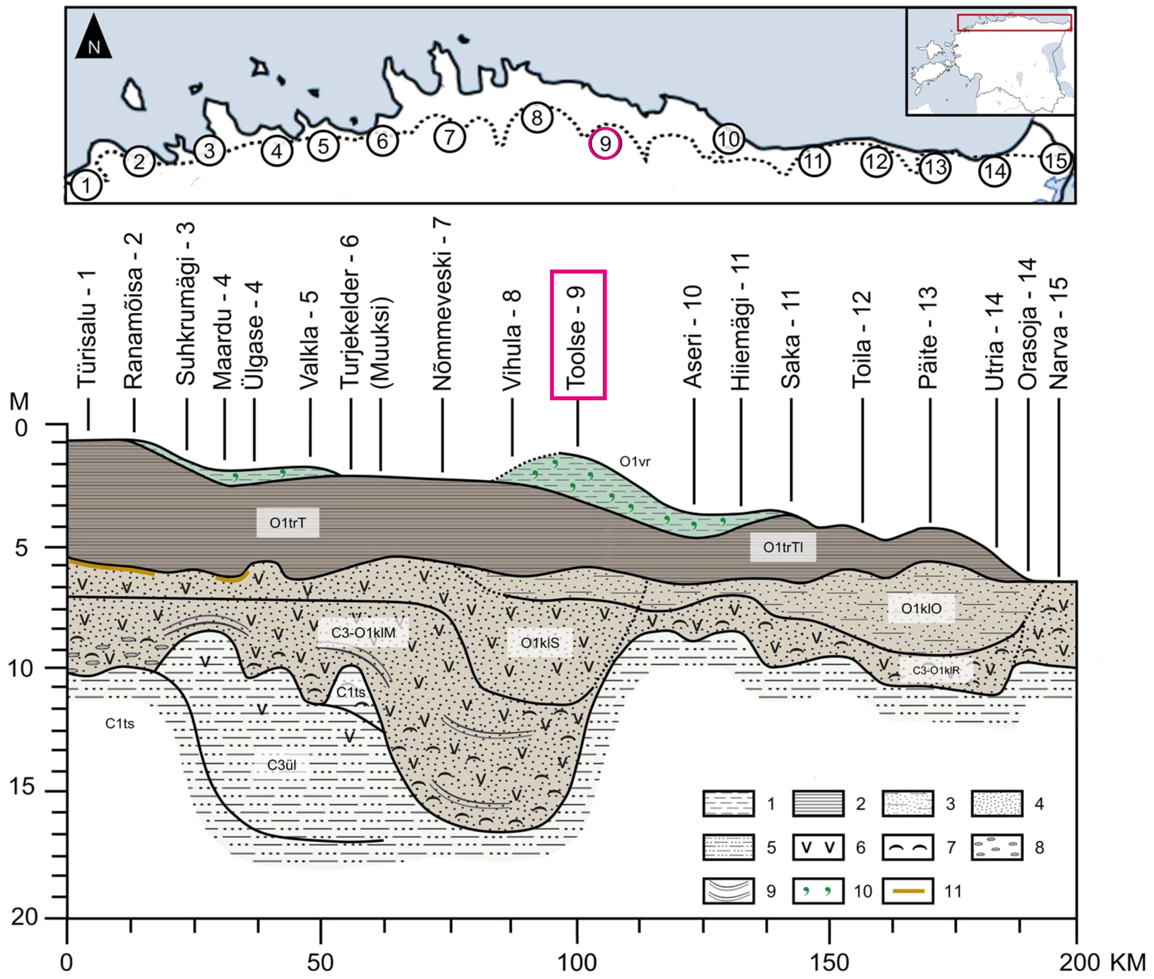

Cross-section of the Tremadocian sedimentary rocks after Heinsalu et al. [5]. 1 - Compact claystone 2 - Kerogenous black shale 'Graptolite argillite'. 3 – Silty sandstone with BS layers. 4 - Sandstone. 5 – Silty sandstone with clays. 6 – Debris of phosphatized brachiopods. 7 – Intact valves. 8 – Phosphatized pebbles. 9 – Clay interbeds. 10 – Glauconite. 11 – Pyrite.

TAL TECH

GEOLOGICAL SETTING AND ANALYZE PLAN

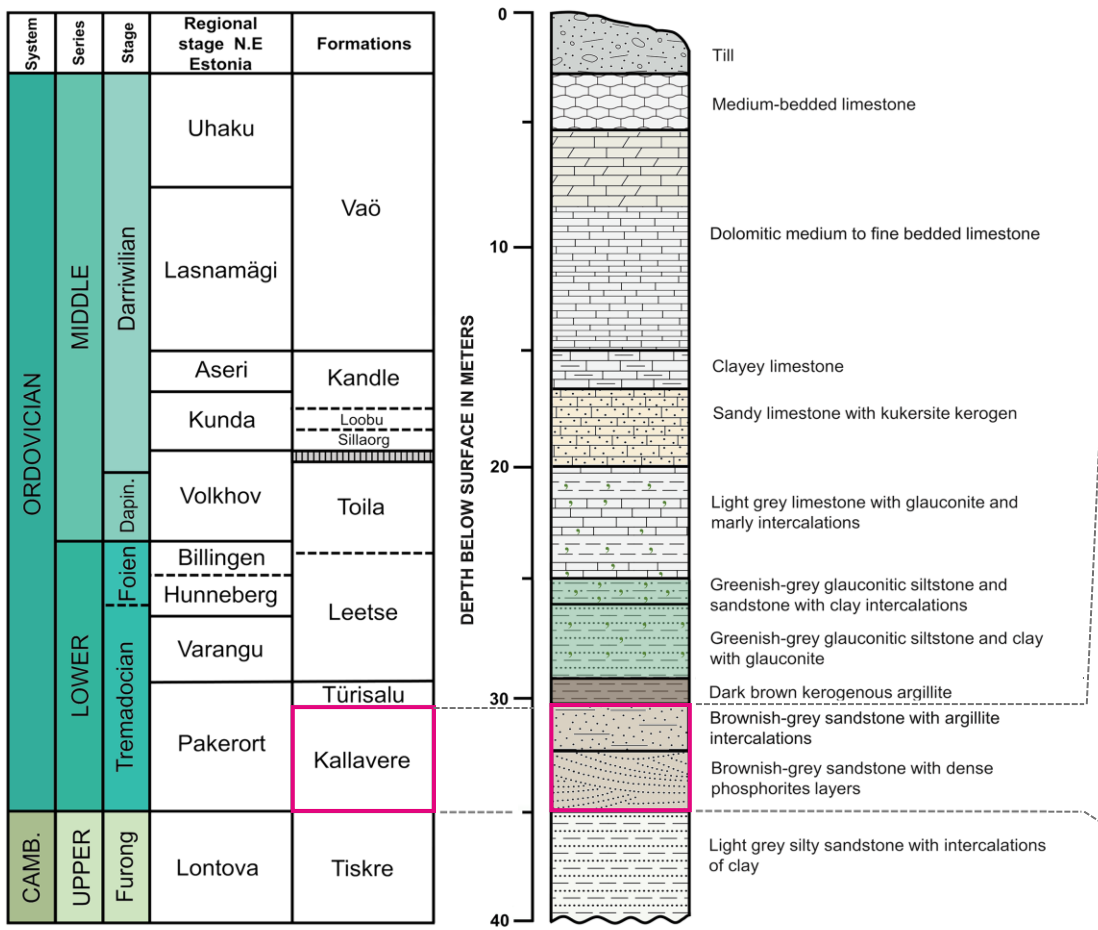

General stratigraphy and cross section of the Toolse deposit, with detail of the Kallavere Formation, regional stratigraphy after Nõlvak et al. [4].

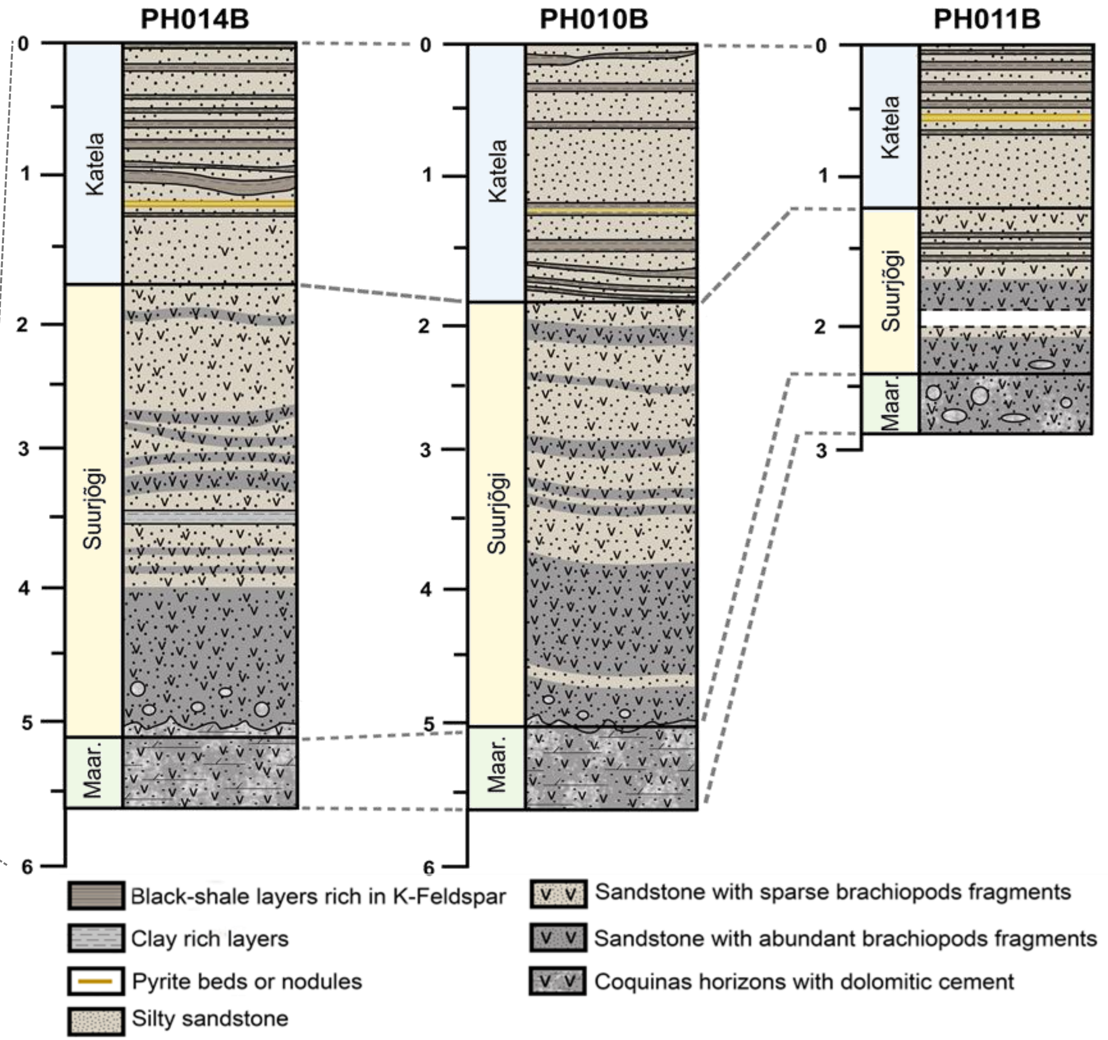

Visual description of the analyzed drill cores, represented in 50cm intervals

- $REE_{SN}+Y_{SN}$ 140 whole-rock and 14 discrete black-shale samples. Development of a general ore model.

MINERALOGY & FEATURES

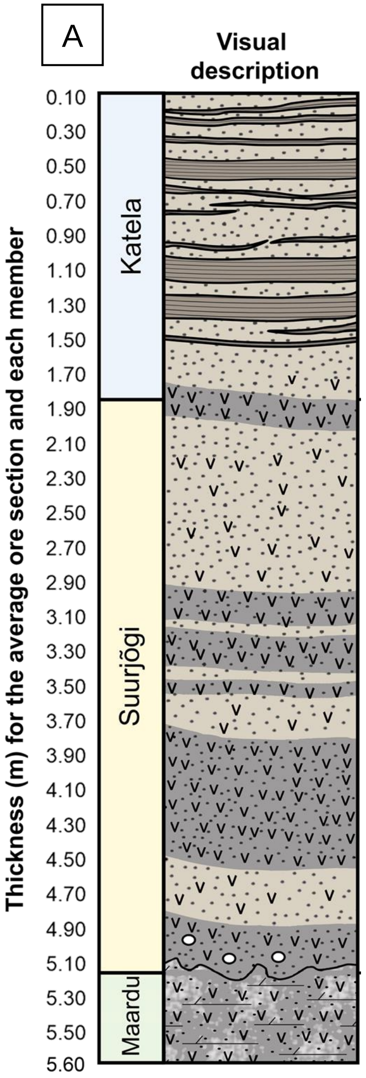

Silty sandstone and low phosphorus content. Occurrence of transgressive black-shale interbeds, with vanadium rich clays, K-feldspars and detrital heavy minerals.

Coarser sandstone, cemented by quartz overgrowth (B.1), with layers of dark shell fragments (B.2)

Horizons, sometime cross-bedded, with downward increasing fragments size and content (C.3)

Phosphatic shell coquinas with pyrite nodules (C.4&5) dolomitic cement (C.6)

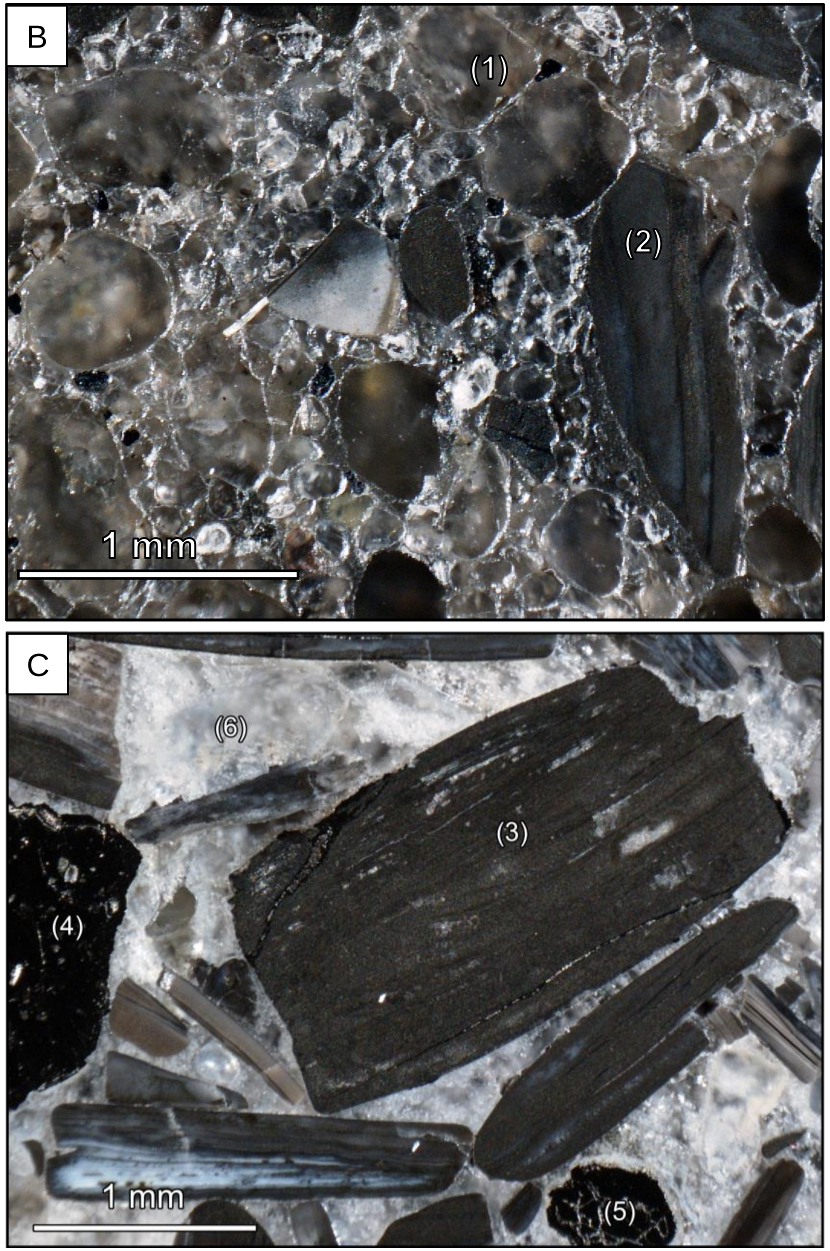

Optical microscopy images of shelly phosphorites

Ore section

MINERALOGY & FEATURES

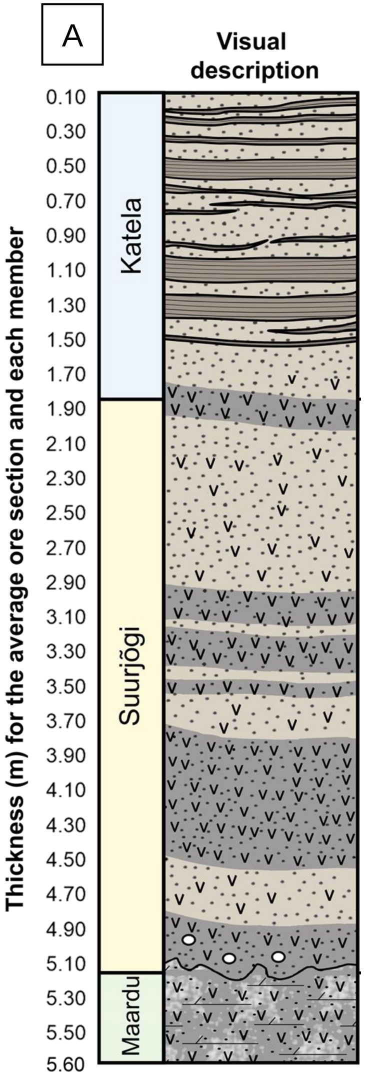

Silty sandstone and low phosphorus content. Occurrence of transgressive black-shale interbeds, with vanadium rich clays, K-feldspars and detrital heavy minerals.

Coarser sandstone, cemented by quartz overgrowth (B.1), with layers of dark shell fragments (B.2)

Horizons, sometime cross-bedded, with downward increasing fragments size and content (C.3)

Phosphatic shell coquinas with pyrite nodules (C.4&5) dolomitic cement (C.6)

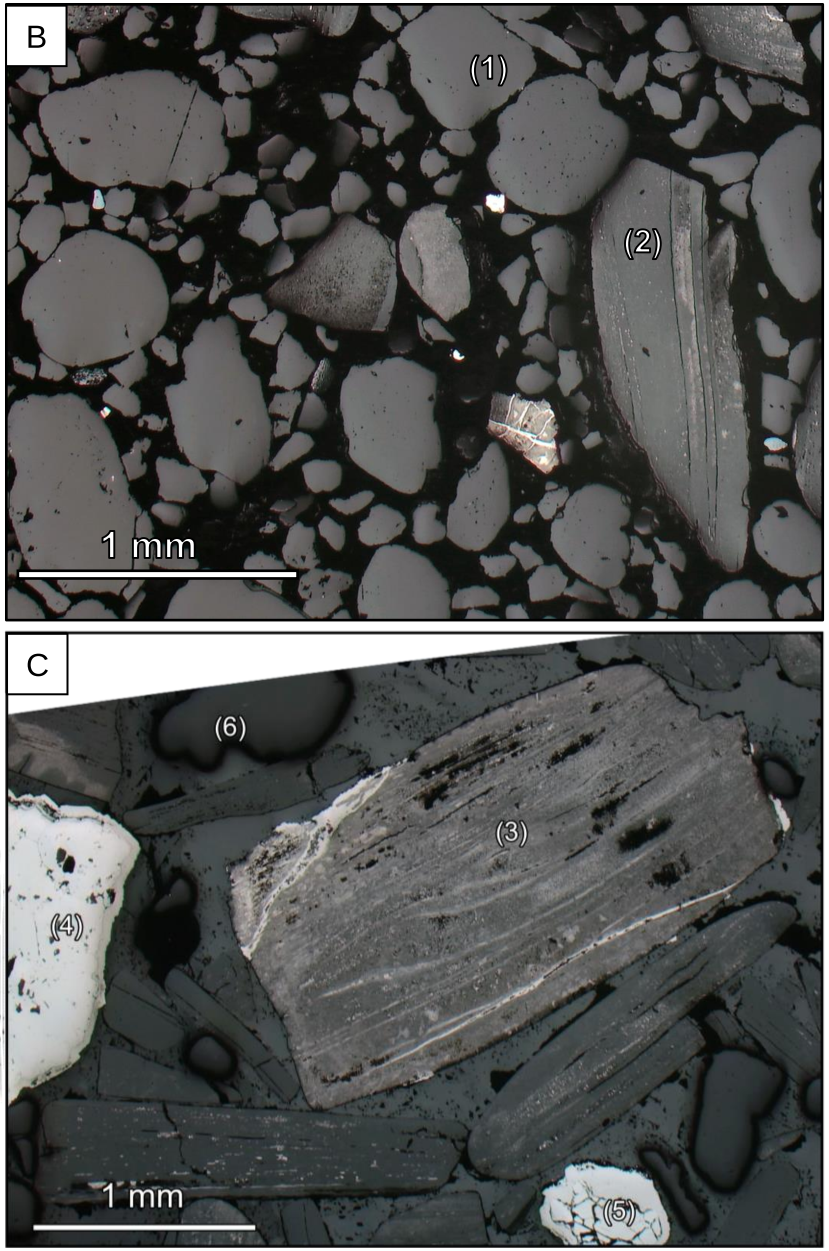

Optical microscopy images of shelly phosphorites

Ore section

MINERALOGY & FEATURES

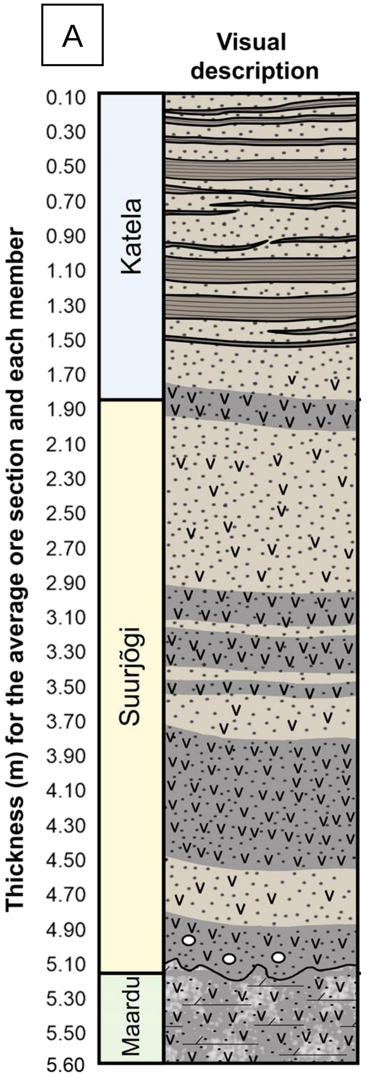

Silty sandstone and low phosphorus content. Occurrence of transgressive black-shale interbeds, with vanadium rich clays, K-feldspars and detrital heavy minerals.

Coarser sandstone, cemented by quartz overgrowth (B.1), with layers of dark shell fragments (B.2)

Horizons, sometime cross-bedded, with downward increasing fragments size and content (C.3)

Phosphatic shell coquinas with pyrite nodules (C.4&5) dolomitic cement (C.6)

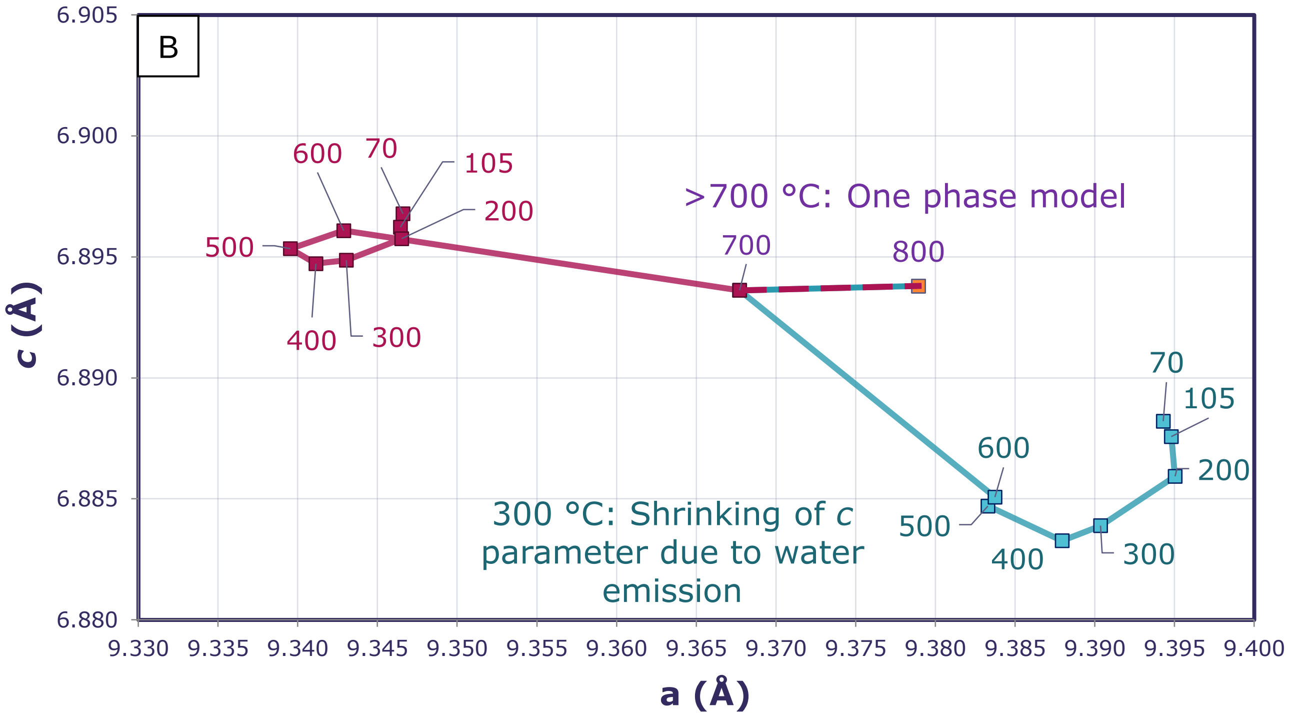

Lattice parameters of different heating steps from High-Temperature XRD experiment on intact shells

C) Occurrence of two phases of low crystallinity apatite :

- A 'biogenic' hydroxyapatite, rich in H_2O and CO_2, unstable phase during burial.
- A stable carbonate fluorapatite (CAF) phase, close to francolite structure:

$$Ca_{10-a-b}Na_{a-}Mg_b(PO_4)_{6-x}(CO_3)_{x-y-z}(CO_3.F)_y(SO_4)_2$$

TAL TECH

REE+Y DISTRIBUTION – GENERAL MODEL TREND WITH DEPTH

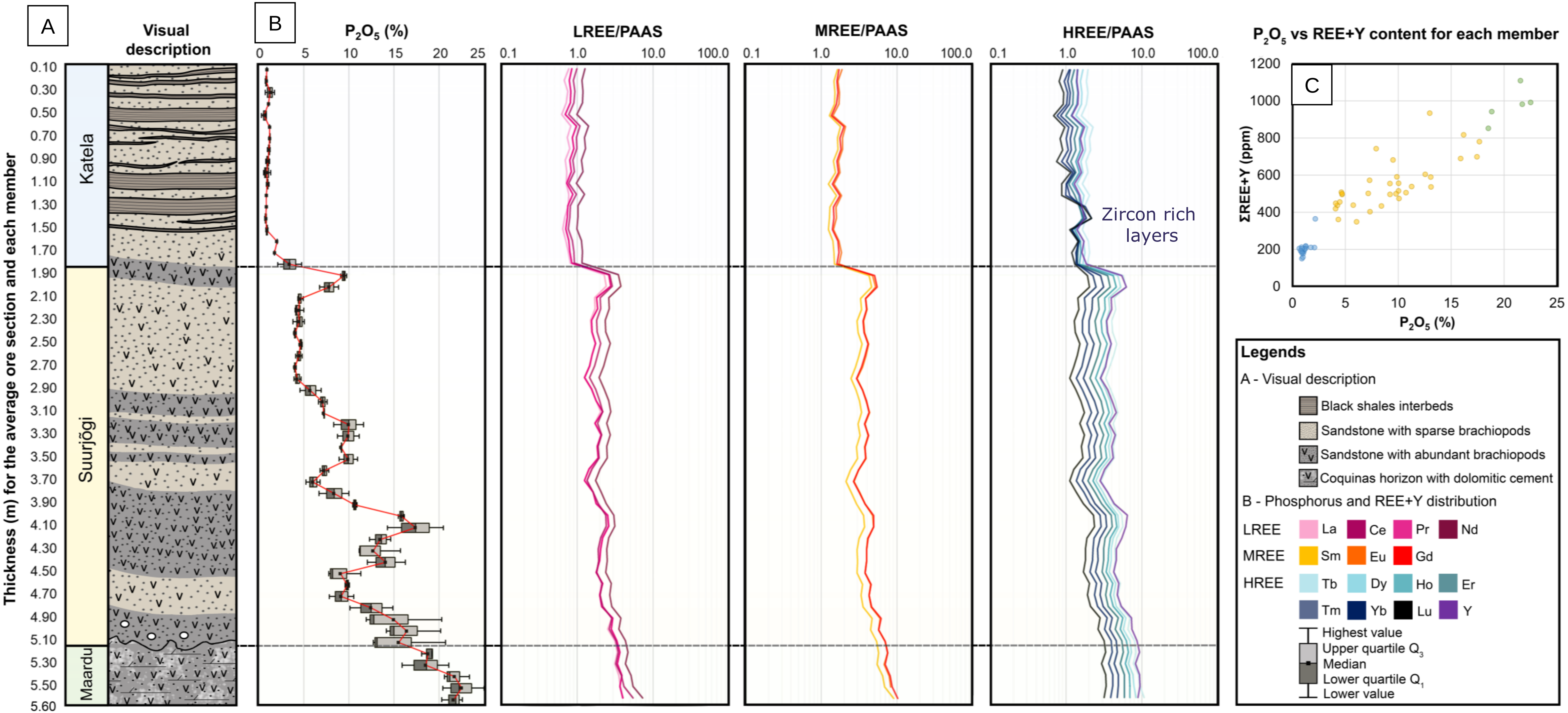

- High correlation between P_2O_5 and ∑REE : apatite as the sole carrier for REE.
- High similarity of trends between the different REEs : Global REE enrichment mechanism(s) and reliable bases for REE-resource calculation.

TAL TECH

REE+Y ENRICHMENT

A) REE+Y enrichment and features

- MREE enrichment and 'bell-shaped' patterns: secondary signature, different from the pristine 'hat-pattern' of coastal bioapatite [6]. High magnitude (11).
- Y positive anomaly: signal of oxic, shallow environment.
- LREE enrichment, especially in the Maardu Member.

B & C) Ce anomalies and implications for depositional and diagenetic redox conditions

- Positive Ce Ω anomalies or no anomalies: not consistent with shallow oxic conditions.
- Correlation between Ce Ω and ∑REE: progressive scavenging after deposition, not driven by redox states.

Average $REE_{SN}+Y_{SN}$ data per 10 cm intervals.
Red doted lines stand for zircon-rich intervals

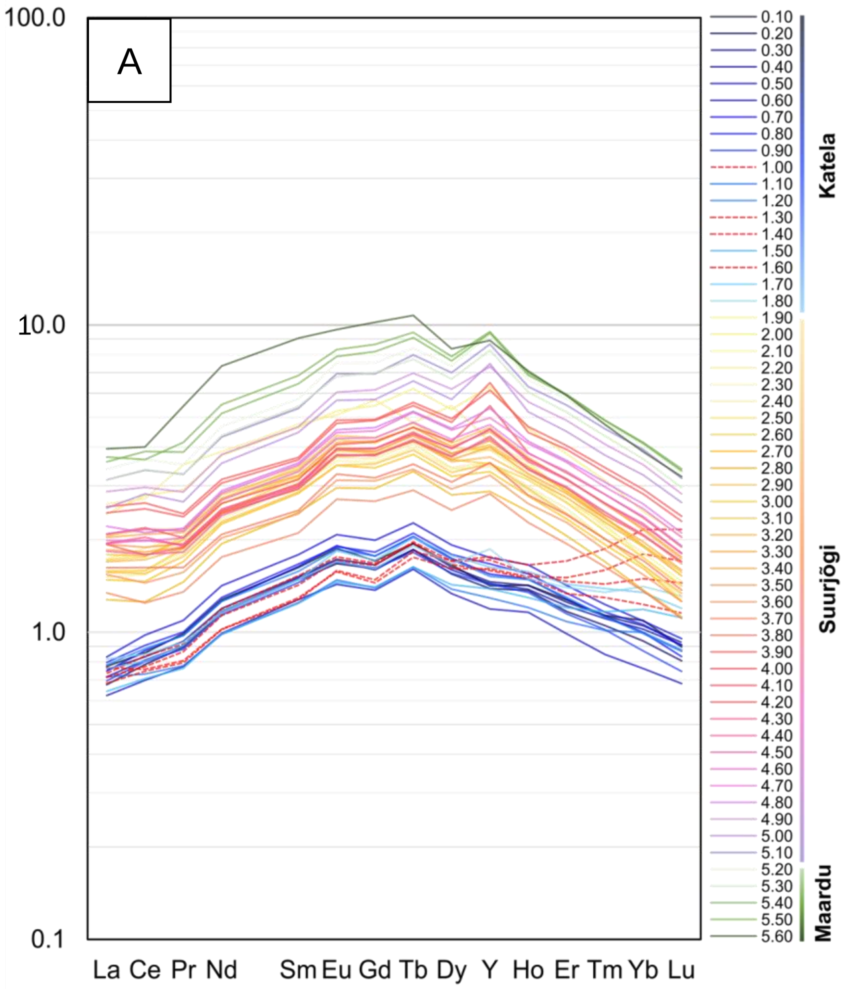

Ce anomaly plot after Bau & Dulski [7]

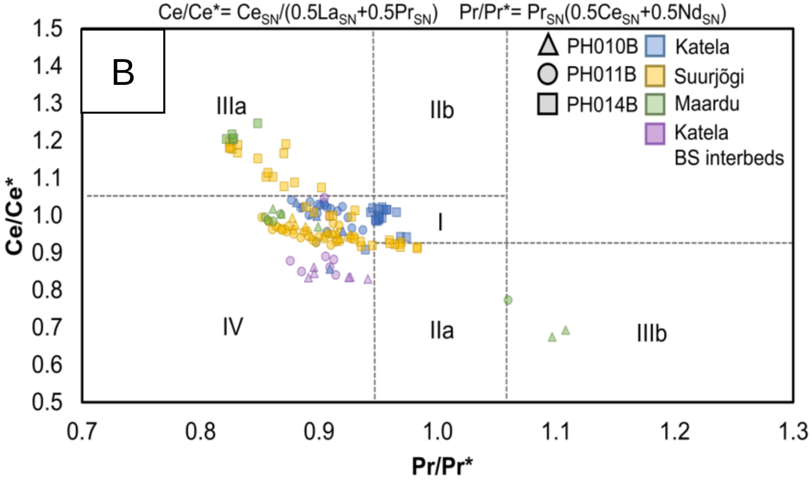

I: No anomaly
IIa: Apparent positive anomaly
IIb: Apparent negative anomaly
IIIa: True positive anomaly
IIIb: True negative anomaly
IV: Positive La-anomaly disguises positive Ce-anomaly

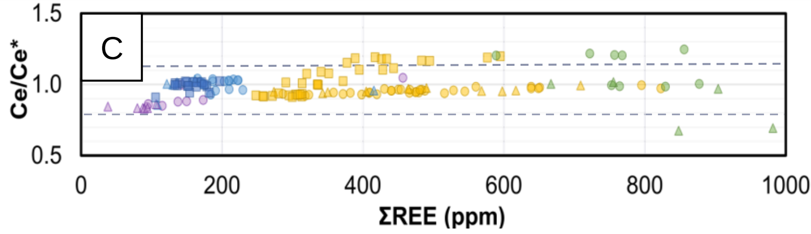

REE+Y ENRICHMENT

A) REE+Y enrichment and features

- MREE enrichment and 'bell-shaped' patterns: secondary signature, different from the pristine 'hat-pattern' of coastal bioapatite [6]. High magnitude (11).
- Y positive anomaly: signal of oxic, shallow environment.
- LREE enrichment, especially in the Maardu Member.

B & C) Ce anomalies and implications for depositional and diagenetic redox conditions

- Positive Ce Ω anomalies or no anomalies: not consistent with shallow oxic conditions.
- Correlation between Ce Ω and ΣREE: progressive scavenging after deposition, not driven by redox states.

Average $REE_{SN}+Y_{SN}$ data per 10 cm intervals. Red doted lines stand for zircon-rich intervals

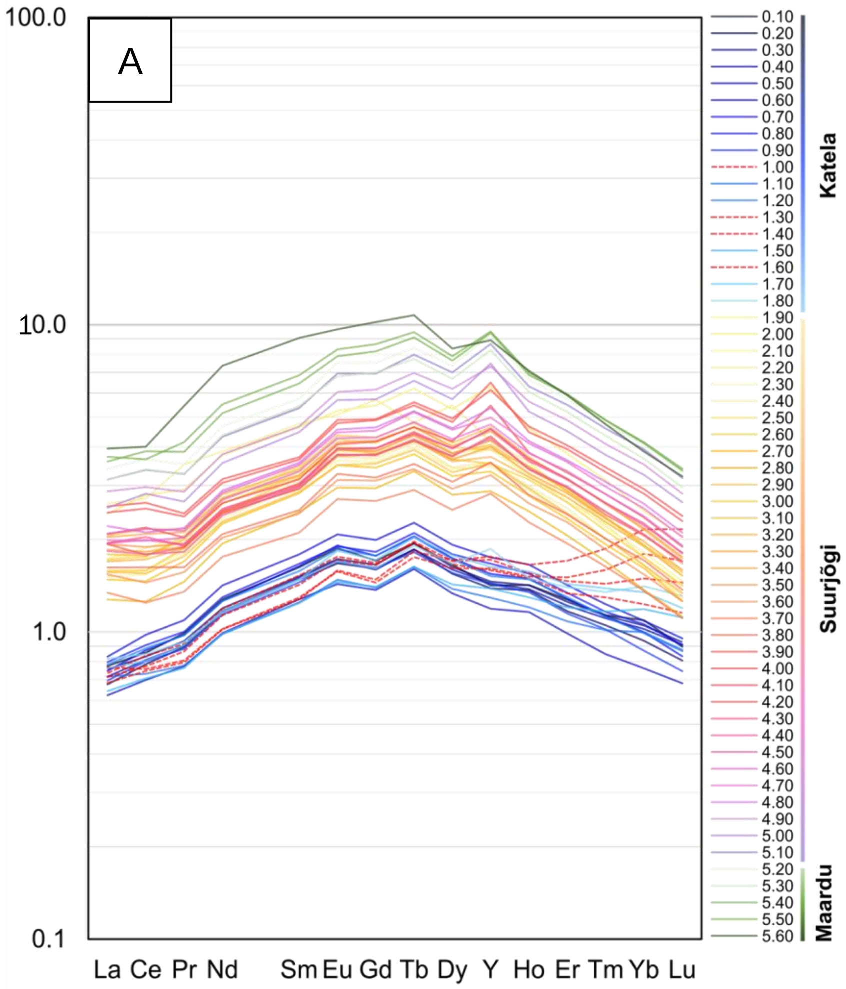

$REE_{SN}+Y_{SN}$ data for all drill cores and BS interbeds

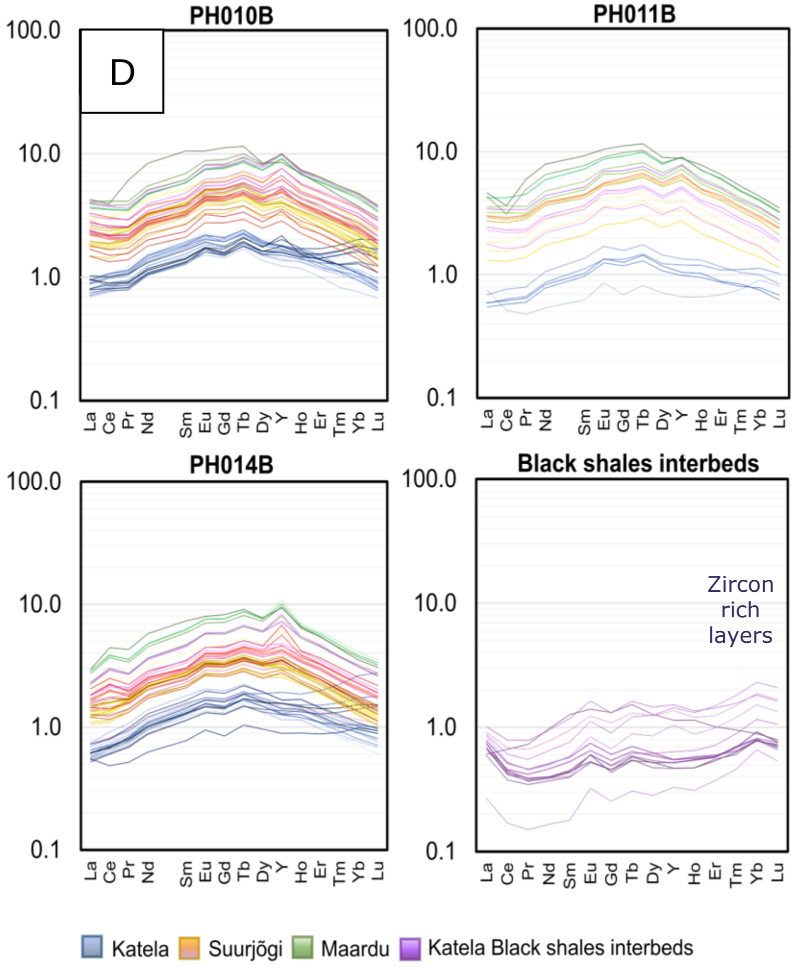

D) Local variations during the sedimentation

- Local variabilities (Ce, Y) in synsedimentary or diagenetic pore water.
- Black-shales with low REE and P content ($P_2O_5 < 2\%$), but with developing bell-shaped pattern : general diagenetic enrichment/overprint.

TAL TECH

REE+Y CARRIERS AND INTAKE

REE+Y intake mechanisms, environment and precursor carriers phases during diagenesis

- A) Trend toward diagenetic enrichment [8].
- B) Bell-shaped index : diagenetic MREE enrichment was at constant intensity and in equilibrium with the pore water [9].

  MREE are primarily carried by Fe-oxyhydroxides [10].
- C) MnO-oxyhydroxides as main contributor of LREE (mainly Ce^{3+}, captured on MnO-oxides surface) content in the shelly phosphorite [11,12].
- D) Slight increase in the $(La/Yb)_{SN}$ ratio with the more REE-rich samples : adsorption as main REE intake mechanism during the diagenesis in authigenic CAF-apatite [13].

Diagnostic ratios of REE+Y and P_2O_5.
Red dots stand for zircon-rich intervals

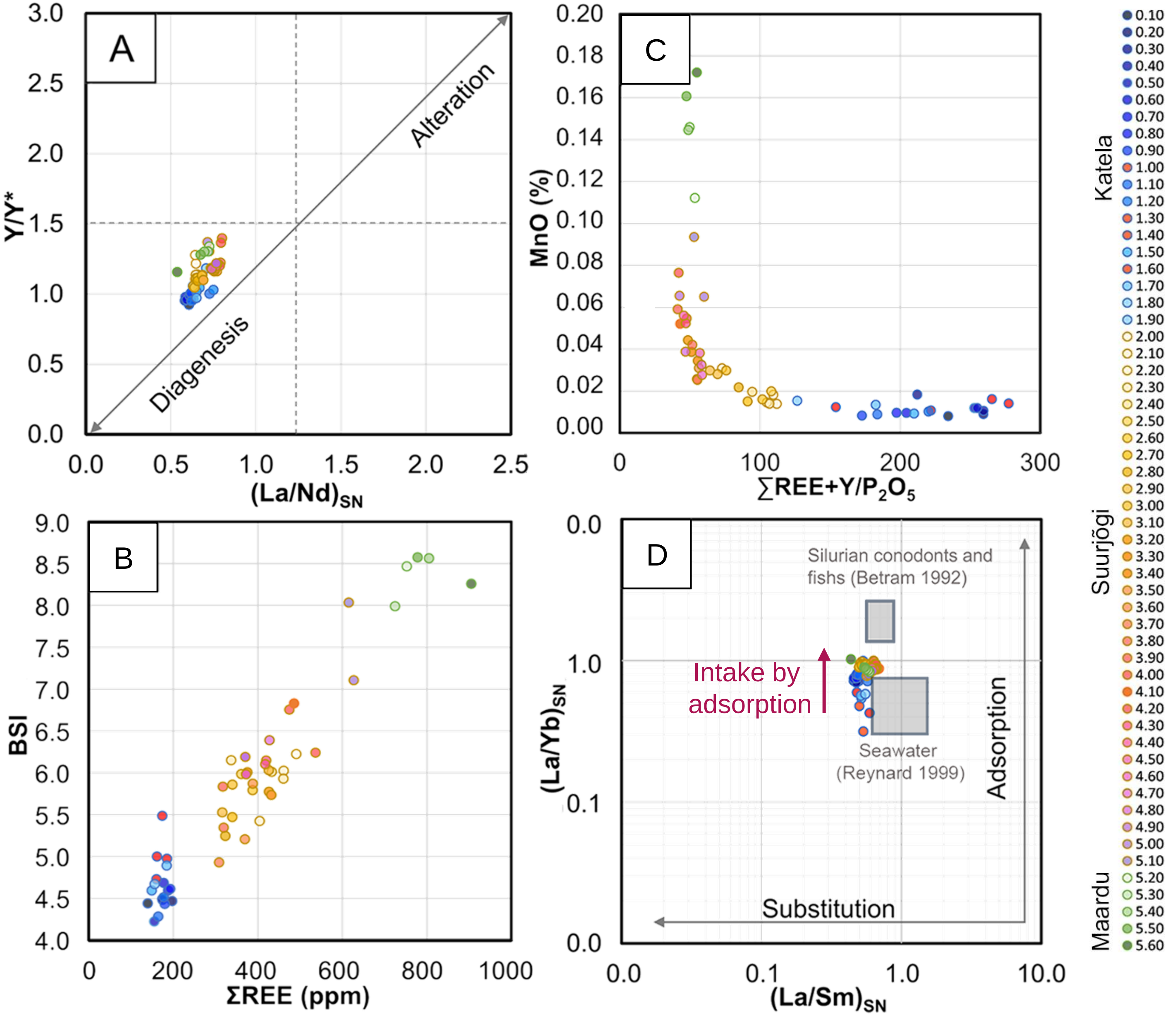

$$BSI = \frac{2 * ([Sm]_{SN} + [Gd] + [Dy]_{SN})}{([La]_{SN} + [Pr]_{SN} + [Nd]_{SN})/3 + ([Ho]_{SN} + [Er]_{SN} + [Tm]_{SN} + [Yb]_{SN} + [Lu]_{SN})/5}$$

TAL TECH

REE+Y CARRIERS AND INTAKE – HISTORICAL DATA & DEPOSITION

Evolution of REE fractionation signals of shelly phosphorite, from deposition to burial in coastal paleosettings

- A) ‘Hat-shaped’ to ‘bell-shaped’ pattern path of shells REE signals :
  - Equilibrium with coastal seawater (1).
  - Deposition in nutrient rich water (2).
  - Intake in equilibrium with diagenetic pore fluids (3).
- B) REE intake by substitution mechanism in non-altered shells :
  - Initial substitution pattern in biogenic hydroxyapatite, in equilibrium with seawater.
  - Superposition of an adsorption-related fractionation pattern in authigenic CAF-apatite during the burial/early diagenesis.

REE Estonian and NW Russian brachiopods and conodonts data from Lécuyer et al. [14], and Grandjean-Lécuyer et al. [15].

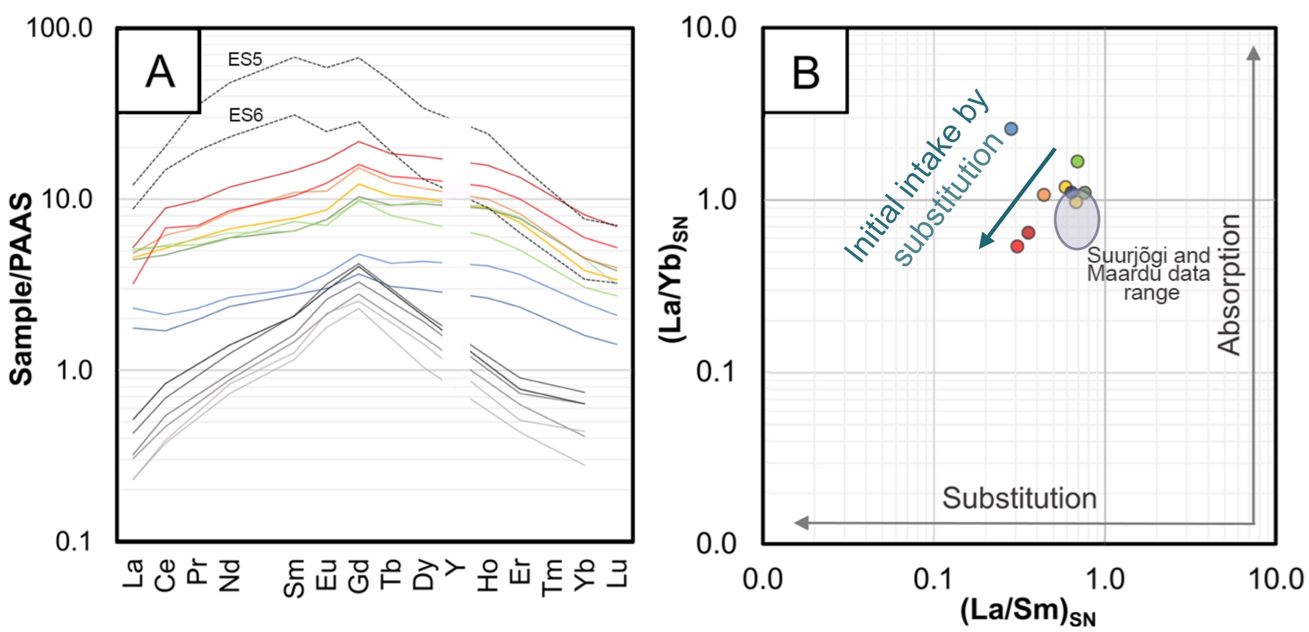

(1) Coastal conodonts data from Grandjean-Lécuyer et al. Cou 23-34a

(2) Estonian and NW Russian non-altered brachiopods data from Lécuyer et al.

(3) Estonian ‘altered’ brachiopods data from Lécuyer et al.

TAL TECH

GENERAL MODEL

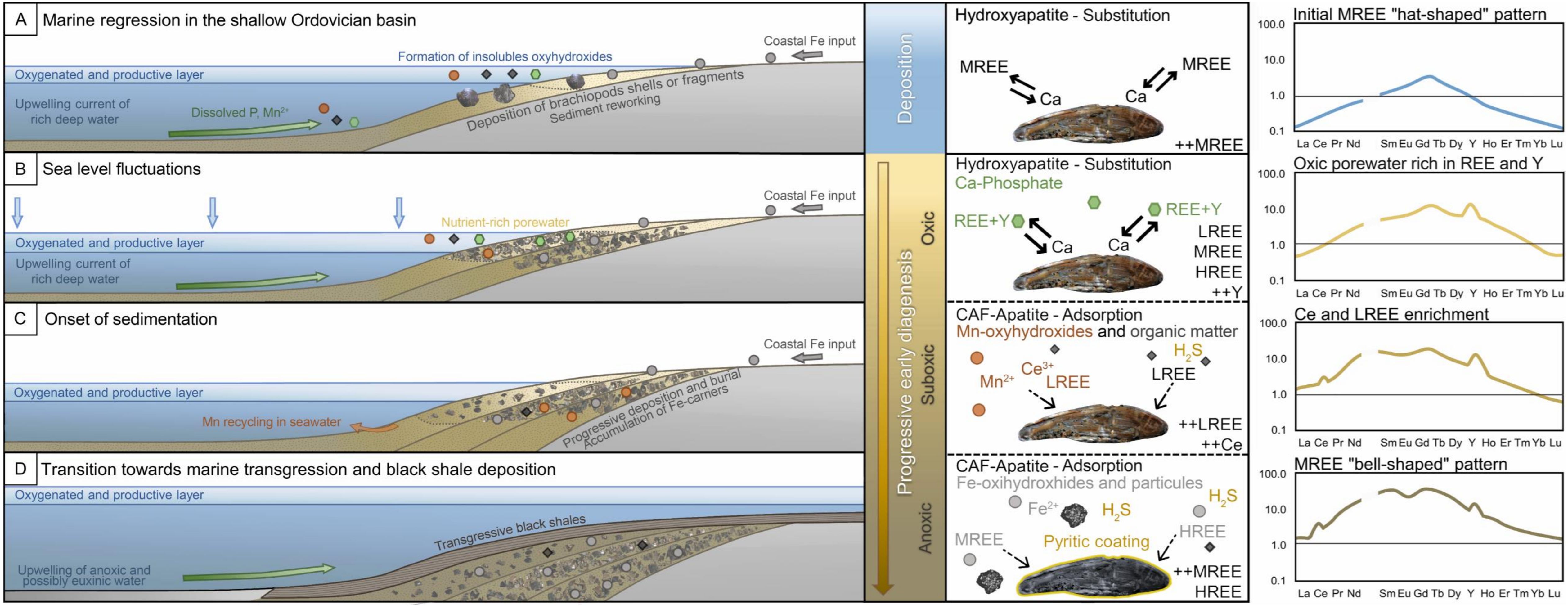

- A. Upwelling of deep-water rich in precursor carrier phases and transport of brachiopods fragments to the near-shore.
- B. Deposition of shells in sediment with oxic nutrient-rich pore water.
- C. Shallow burial and attainment of suboxic conditions due to steep redox gradient. Transformation of hydroxyapatite in CAF-apatite. Desorption of Mn-oxyhydroxides and release of LREE. Accumulation of Fe^{2+} and MREE in FeS_x.
- D. Development of anoxic conditions during the early-diagenesis. Release of MREE and acquisition of ‘bell-shaped’ pattern.

CONCLUSION, UPCOMING STUDIES & PERSPECTIVES

Conclusion

- Multistage nature of REE+Y enrichment process within the shelly phosphorite resources of the Kallavere Formation.
- REE scavenging predominantly controlled by adsorption to authigenic CAF-apatite during two consequent early-diagenetic enrichment stages.

Upcoming studies and perspectives

- MLA and EMPA systematic profiles investigations for ore processing and modelling.
- LA-ICP-MS mapping detailed REE+Y distribution in shells.
- High-resolution analyses for Tremadocian paleosettings, from phosphorites to black-shales.
- Comparison to other organophosphatic deposit / upwelling-related deposits (Permian and Cambrian deposits, Namibian shelly deposits).

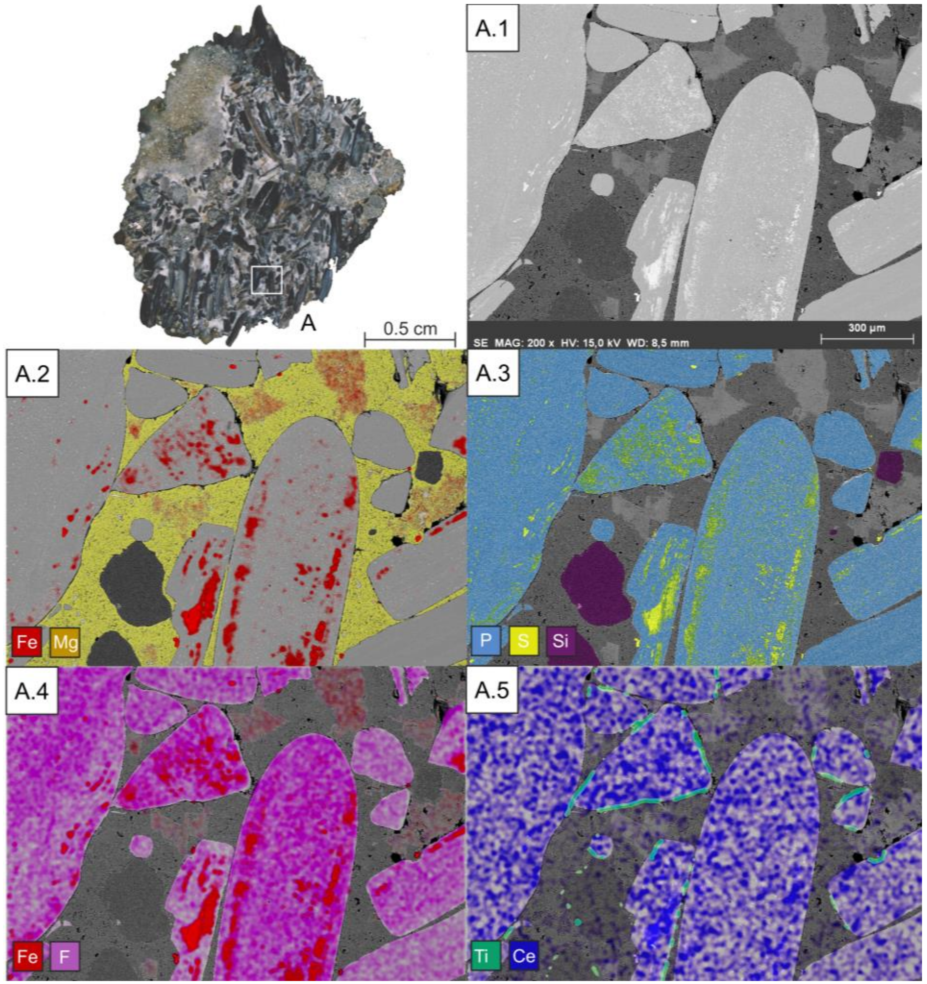

Example of FE-SEM element mapping tests and core section of the transition layers between black-shales and phosphorites

TAL TECH

REFERENCES

[1] L. R. Cocks and T. Torsvik, "Earth geography from 500 to 400 million years ago: a faunal and palaeomagnetic rievew," Journal of the Geological Society, vol. 159, pp. 631-644, 2002.

[2] L. E. Popov, J.-J. Alvaro, L. E. Holmer, H. Bauert, M. G. Pour, A. V. Dronov, O. Lehnert, O. Hints, Z. Zhang and Z. Zhang, "Glendonite occurrences in the Tremadocian of Baltica: first Early Palaeozoic evidence of massive ikaite precipitation at temperate latitudes," Scientific Reports, vol. 9, 2019.

[3] H. Bauert, A. Soesoo and S. Hade, "Strategic raw materials of Estonia," in Eesti strateegilised maavarad, Rakvere, 2015.

[4] J. Nõlvak, O. Hints and P. Männik, "Ordovician timescale in Estonia: recent developments," Proceedings of the Estonian Academy of Sciences, vol. 55, pp. 95-108, 2006.

[5] H. Heinsalu and R. Raudsep, "Lithology of the Kallavere formation on the North-Estonian Klint (Part I- Paldiski Kunda area)," Bulletin of the Geological Survey of Estonia, vol. 8, no. 1, pp. 20-31, 1998.

[6] C. Lécuyer, B. Reynard and P. Grandjean, "Rare earth element evolution of Phanerozoic seawater recorded in biogenic apatites," Chemical Geology, vol. 204, no. 1-2, pp. 63-01, 2004.

[7] M. Bau and P. Dulski, "Distribution of Yttrium and Rare-Earth Elements in the Penge and Kuruman Iron Formation, Transvaal Supergroup, South Africa," Precambrian Research, no. 79, pp. 37-55.

[8] G. A. Shields, P. Stille, “Diagenetic constraints on the use of cerium anomalies as palaeoseawater redox proxies: an isotopic and REE study of Cambrian phosphorites”, Chemical Geology, vol. 175, issue 1-2, 2001.

[9] R. Totsevin, G. A. Shields, G. M. Tarbuck, H. Tianchen, M. O. Clarkson and R. A. Wood, "Effective use of cerium anomalies as a redox proxy in carbonate-dominated marine settings," Chemical Geology, vol. 438, pp. 146-162, 2016.

[10] A. Ohta and I. Kawabe, "REE(III) adsorption onto Mn dioxide (delta-MnO_2) and Fe oxyhydroxide: Ce(III) oxidation by delta-MnO_2," Geochimica et Cosmochimica Acta, vol. 65, no. 5, pp. 695-703, 2001.

[11] B. Reynard, C. Lécuyer and P. Grandjean, "Crystal-chemical controls on rare-earth element concentrations in fossil biogenic apatites and implications for paleoenvironmental reconstructions," Chemical Geology, vol. 155, no. 3-4, pp. 233-41, 1999.

[12] Determination of the oxidation state of cerium in rocks by Ce LIII-edge X-ray absorption near-edge structure spectroscopy

[13] B. A. Haley, G. P. Klinkammer and J. McManus, "Rare earth elements in pore waters of marine sediments," Geochimica et Cosmochimica Acta, vol. 68, no. 6, pp. 1265-1279, 2004.

[14] C. Lécuyer, P. Grandjean, J.-A. Barrat, J. Nolvak, C. Emig, F. Paris and M. Robardet, "$\delta^{18}O$ and REE contents of phosphatic brachiopods: a comparison between modern and lower Paleozoic populations," Geochimica et Cosmochimica Acta, vol. 62, no. 14, pp. 2429-2436, 1998

[15] P. Grandjean-Lécuyer, R. Feist and N. Albarède, "Rare earth elements in old biogenic apatites" Geochimica et Cosmochimia Acta, vol. 57, pp. 2507-2514, 1993.

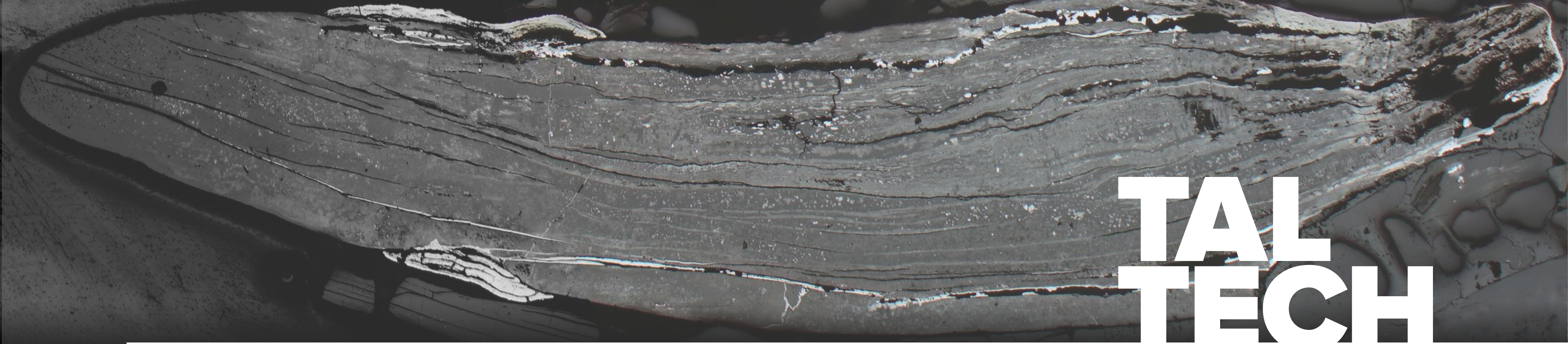

THANK YOU !

Special thanks to: Rutt HINTS, Siim PAJUSAAR, Toivo KALLASTE, Mawo N'DIAYE, Kristjan URTSON, Andre GREGOR & Nthati MONEI

sophie.graul@taltech.ee

This work was supported by the Estonian Research Council project RESTA23

THE GEOLOGICAL SOCIETY OF AMERICA®
CONNECTS 2022
9–12 October
Denver, Colorado, USA
& Online Everywhere

TALLINN UNIVERSITY OF TECHNOLOGY

Estonian Research Council